REVISED

SHORT COMMUNICATON

Heterogeneity in ERK activity as visualized by in vivo FRET imaging of mammary tumor cells developed in MMTV-Neu mice

Running Title: Heterogeneity in ERK activity in mammary tumor cells

Yuka Kumagai,[1] Honda Naoki,[4] Eiji Nakasyo,[5] Yuji Kamioka,[2,3] Etsuko Kiyokawa,[6] and Michiyuki Matsuda[1, 2]*

[1]Department of Bioimaging and Cell Signaling, Graduate School of Biostudies, [2]Department of Pathology and Biology of Diseases, Graduate School of Medicine,[3]Imaging Platform for Spatio-Temporal Information, Graduate School of Medicine and [4]Innovative Techno-Hub for Integrated Medical Bio-Imaging, Kyoto University, Kyoto 606-8501, Japan. [5]Life & Industrial Products Development Department 1, R&D Division, Olympus Corporation, Hachioji, Japan. [6]Department of Oncologic Pathology, Kanazawa Medical University, 1-1 Daigaku, Uchinada, Kahoku-gun, Ishikawa 920-0293, Japan

* Correspondence: matsuda.michiyuki.2c@kyoto-u.ac.jp

Key Words: Breast cancer, ERK, FRET biosensor, in vivo imaging

ABSTRACT

Human epidermal growth factor receptor 2 (HER2)/Neu, which is overexpressed in about 30% of human breast cancers, transduces growth signals in large part via the Ras-Raf-MEK-ERK pathway. Nevertheless, it is a matter of controversy whether high ERK activity in breast cancer tissues correlates with better or worse prognosis, leaving the role of ERK activity in the progression of breast cancers unresolved. To address this issue, we live-imaged ERK activity in mammary tumors developed in mouse mammary tumor virus (MMTV) - Neu transgenic mice, which had been crossed with transgenic mice expressing a FRET biosensor for ERK. Observation of the tumor by two-photon microscopy revealed significant heterogeneity in ERK activity among the mammary tumor cells. The level of ERK activity in each cell was stable up to several hours, implying a robust mechanism that maintained the ERK activity within a limited range. By sorting the mammary tumor cells based on their ERK activity, we found that ERK^{high} cells less efficiently generated tumorspheres in vitro and tumors in vivo than did ERK^{low} cells. In agreement with this finding, the expressions of the cancer-stem-cell markers CD49f, CD24, and CD61 were decreased in ERK^{high} cells. These observations suggest that high ERK activity may suppress the self-renewal of mammary cancer stem cells.

INTRODUCTION

Cancer cells display phenotypic and functional heterogeneity. The concept of cancer stem cells (CSCs)/tumor initiating cells (TICs) is a representative example of such heterogeneity within a single tumor [1]. CSCs/TICs have the ability to self-renew and generate a diverse range of tumor cells, and thus serve as promising anti-cancer drug targets [2]. Nevertheless, methods to study CSCs/TICs in vivo are limited because the identification of CSCs/TICs depends on the expression of cell surface markers.

Human epidermal growth factor receptor 2 (HER2)/Neu is overexpressed in some 30% of breast cancers and associated with poor prognosis [3]. It has been suggested that HER2/Neu may

regulate the CSC/TIC property. In HER2-overexpressing carcinoma cell lines, cells with a CSC/TIC property presented increased HER2 levels compared with the bulk cell population [4]. HER2 overexpression in normal mammary epithelial cells increases the proportion of stem and progenitor cells [5]. In line with these observations, it has been shown that the effects of HER2 overexpression on breast cancer stem cells are blocked by the HER2 inhibitor trastuzumab [4, 5]. Moreover, overexpression of the polycomb protein EZH2, which has been linked to breast cancer progression, causes RAF1 amplification and, thereby, ERK activation to promote CSC/TIC expansion [6].

The receptor-type tyrosine kinases, including HER2/Neu, transduce growth signals in large part via the Ras-Raf-MEK-ERK pathway [7]. In mouse mammary tumor virus (MMTV)- Neu transgenic mice, which are widely used as a mouse model of HER2/Neu-positive luminal-type breast cancer [8, 9], ERK regulates the self-renewal of mammary stem and progenitor cells by upregulation of cyclin D1 kinase activity [10] and contributes to malignancy by increasing the activity of the Notch pathway [11]. ERK also regulates many other cancer cell phenotypes, such as invasion and metastasis [7]. In agreement with these observations, high ERK activity in breast cancer tissues has been shown to correlate with poor prognosis of patients [12]. It has also been reported that activation of the ERK pathway drives resistance to paclitaxel [13].

Surprisingly, however, in some clinical studies high ERK activity in breast cancer tissues is associated with improved survival [14-16]. This seemingly contradictory observation might involve the inhibitory effect of ERK on the self-renewal of stem cells [17, 18]. Even though the inhibitory role of ERK on maintenance of the undifferentiated state is cell type-specific [19], it should be of great concern whether ERK plays a positive or negative role in the self-renewal of CSCs/TICs of mammary tumors, considering the fact that many anti-cancer drugs target the HER2/Neu-Ras-ERK pathway. To answer this question, we visualized the ERK activity in mammary tumors developed in MMTV- Neu transgenic mice that had been crossed with transgenic mice expressing a Förster resonance energy transfer (FRET) biosensor for ERK [20]. Observation of the transgenic mice by two-photon (2P) microscopy revealed significant

heterogeneity in ERK activity among the primary breast cancer cells. By sorting the mammary tumor cells based on their ERK activity, we found that ERK^{high} cells generated tumorspheres in tissue culture and tumors after orthotopic implantation less efficiently than did ERK^{low} cells.

RESULTS AND DISCUSSION

Heterogeneity in ERK activity as visualized by in vivo FRET imaging

To study the role of ERK activity in mammary tumors, we crossed MMTV-$Neu^{+/+}$ mice with $EKAREV^{+/-}$ mice, which express a FRET biosensor for ERK, EKAREV [21]. With $EKAREV^{+/-}$ mice, ERK activity in mouse tissues can be visualized by the YFP/CFP ratio image (Supplementary Fig. S1A). The obtained $EKAREV^{+/-}$/MMTV-$Neu^{+/-}$ mice were indistinguishable from the parent MMTV-$Neu^{+/-}$ mice in size, the susceptibility to mammary tumor development, and the histological appearance of the developed tumors. We first observed normal mammary glands of $EKAREV^{+/-}$ mice by 2P microscopy (Fig. 1A). The EKAREV biosensor was expressed both in luminal epithelial cells and myoepithelial cells. The level of ERK activity was higher in myoepithelial cells than luminal epithelial cells. Tissue autofluorescence of mammary tissues was negligible in our experimental setup (Supplementary Fig. S1B, C).

The $EKAREV^{+/-}$/MMTV-$Neu^{+/-}$ mice developed mammary tumors from 24 weeks after birth. We found that tumor cells exhibited significant heterogeneity in ERK activity without forming any clusters with similar activity levels (Fig. 1B). The standard deviations of the FRET/CFP ratio of luminal epithelial cells and mammary tumors were 0.069 and 0.13, respectively (Fig. 1A, B). There was no correlation between the FRET signal and the expression level of the biosensor, suggesting that the divergence in the FRET signal of mammary tumor cells indeed reflected the heterogeneity in the ERK activity (Fig. 1C). We confirmed the heterogeneity in the ERK activity by immunostaining with an anti-phospho-ERK antibody (Fig. 1D).

To examine whether such diversity in ERK activity was caused by temporal noise or population noise, the mammary tumor cells were live-imaged for six hours. The ERK activities relative to the average for the cell population did not change remarkably in most cells during the course of observation, suggesting that each tumor cell maintained ERK activity homeostasis within a limited range by means of a robust mechanism (Figure 1E, Supplementary Fig. S1D).

Real-time pharmacodynamics of anti-cancer drugs against ERK activity in the primary and secondary tumors

The heterogeneity in the ERK activity among tumor cells inspired us to examine its biological meaning. To investigate this issue, mice bearing the mammary tumors were administered with several anti-cancer drugs. To gain insight into the role of microenvironments, in addition to the primary mammary tumors (P0) we also used passaged mammary tumors (P1), which appeared in one month after the injection of the primary tumor into the mammary fat pad of syngeneic FVB mice. The MEK inhibitor PD0325901 immediately suppressed ERK activity in both the P0 mammary tumor cells and the P1 mammary tumor cells with a half-time of ca. 10 min (Fig. 2A, B). We observed no remarkable differences in the response to PD0325901 between cells close to and those remote from the blood vessels, which were visualized by Qtracker 655 co-injected with the reagents. Notably, the decrease in ERK activity was larger in cells with higher ERK activity than in cells with lower ERK activity (Supplementary Fig. S2A). The low-ERK-activity cells in the P0 tumors appeared to be the least-responsive cell population. Lapatinib, a dual tyrosine kinase inhibitor against epidermal growth factor receptor (EGFR) and epidermal growth factor receptor 2 (HER2), gradually decreased the ERK activity from 10 min after injection in both the P0 mammary tumor cells and the P1 mammary tumor cells (Fig. 2C, D). Again, the low-ERK-activity cells in the P0 tumors responded to Lapatinib least efficiently (Supplementary Fig. S2A). To examine whether the delay might have been caused by the

difference in the pharmacokinetics, we examined the effect of PD0325901 and Lapatinib in vitro with primary mammary tumor cells derived from the transgenic mice (Supplementary Fig. S2B). As observed in vivo, ERK activity in the Lapatinib-treated cells started decreasing with ca. 5 minutes delay, suggesting that the delay was caused by the sensitivity of the tumor cells to Lapatinib. With the in vitro tumor cells, we also examined the response of mammary tumor cells to EGF. In contrast to the response to the inhibitors, any significant correlation was not observed between the basal ERK activity and the EGF-induced increment (Supplementary Fig. S2C). Taken together, these results imply that the heterogeneity in ERK activity in mammary tumor cells may contribute to the difference in the sensitivity to anti-cancer drugs.

In vivo imaging of protein kinase activity by 2P microscopy has opened a new window for the assessment of pharmacodynamics. With transgenic mice expressing FRET biosensors, the effect of an MEK inhibitor on the ERK activity of neutrophils or the effect of a cAMP analogue on the PKA activity of muscles and neurons has been video-imaged in living mice [21]. More recently, the effect of dasatinib on Src activity has also been visualized with subcutaneously implanted pancreatic cancer cells that stably express a FRET biosensor for Src [22]. Here, we showed the drug sensitivity of the mammary tumors developed in MMTV-Neu transgenic mice. We chose PD0325901 and Lapatinib, which are a non-ATP-competitive MEK inhibitor under phase I trial [23] and a dual tyrosine kinase inhibitor of EGFR and HER2 in clinical use [24], respectively. Upon intravenous injection of inhibitors of MEK or HER2, the ERK activity decreased more significantly in high-ERK-activity cells than in low-ERK-activity cells (Fig. 2). Based on this observation, we may be able to speculate that the inhibitors of the HER2/Neu-ERK pathway are less effective for treatment of low-ERK-activity cells.

Decreased tumorsphere formation efficiency and expression of cancer stem cell markers in tumor cells with high ERK activity

To elucidate the role of the heterogeneity of ERK activity among mammary tumor cells, we sorted the cells based on their ERK activity (Fig. 3A). A fluorescent dye that accumulates in dead cells, 7AAD, was included to select for live cells. After selecting single living cells with the forward scatter and side scatter signals, biosensor-expressing cells were identified by the CFP and YFP signals. For cell sorting, the FRET/CFP ratio was used as the index of FRET efficiency as in 3D imaging. Mammary tumor cells in the highest and lowest decile with respect to the FRET/CFP ratio were named the ERK^{high} and ERK^{low} populations, respectively (Fig. 3A). We next compared the biological activity by a tumorsphere formation assay (Fig. 3B). The ERK^{high} population exhibited lower tumorsphere formation efficiency ($0.3 \pm 0.2\%$) compared with the ERK^{low} population ($1.3 \pm 0.2\%$). To understand the role of ERK in tumorsphere formation, we followed the ERK activity of ERK^{high} and ERK^{low} cell populations in vitro. The fraction of high-ERK-activity cells in the ERK^{high} population decreased within nine days to the level of those of the ERK^{low} population (Supplementary Fig. S3A). Timelapse imaging revealed that the high-ERK-activity cells died within three days (Supplementary Fig. S3B), implying that the low tumorsphere formation efficiency of ERK^{high} cells is at least partially attributable to the vulnerability of ERK^{high} cell. The ERK^{high} and ERK^{low} populations were further analyzed by an in vivo transplantation assay (Fig. 3C). Again, the ERK^{high} population yielded tumors less efficiently than did the ERK^{low} population. Because the tumorsphere formation assay and the transplantation assay were used to examine the stem cell property of cancer cells, these results strongly suggested that high ERK activity may suppress the stemness of mammary tumor cells.

To explore this possibility, we examined the expression of mammary stem cell markers on the ERK^{high} and ERK^{low} cell populations. As reported previously [25, 26], a large portion of the MMTV-Neu tumor cells expressed three mammary stem cell markers, CD49f, CD24, and CD61 (Fig. 3D). We found that $CD61^{-}$/$CD49f^{-}$ cells or $CD24^{-}$/$CD49f^{-}$ cells were significantly increased in the ERK^{high} population, suggesting that high ERK activity may suppress the stem cell property of mammary tumor cells. The percentage of $CD61^{-}$/$CD49f^{-}$ cells or

$CD24^{-}/CD49f^{-}$ cells in the ERK^{high} population varied depending on the mouse age, but the pattern was similar in multiple mice (N = 3), showing a reproducible decrease in $CD61^{-}/CD49f^{-}$ cells or $CD24^{-}/CD49f^{-}$ cells in the ERK^{high} population of MMTV-Neu mammary tumor cells.

Finally, we attempted to increase mammary tumor cells bearing the stem cell property by the pretreatment of mice bearing the tumors with the MEK inhibitor. Against our expectation, we failed to observe the decrease in the ERK activity of P0 mammary tumor cells by the daily administration of the MEK inhibitor PD0325901 (Fig. 4A). The discrepancy between the data by FRET imaging (Fig. 2) and the anti-phospho-ERK immunoblotting could be explained by several reasons. First, the variation in the ERK activity of each tumor could be greater than the effect of PD0325901 on each tumor. Second, the daily administration of PD0325901 to the tumor-bearing mice could render the tumor cells resistant to this compound. Third, the FRET biosensor detects the phosphorylation level of the ERK substrates; whereas anti-phospho-ERK immunoblotting detects the phosphorylation of ERK.

Notably, however, the ERK activity in each tumor correlated inversely with the expression levels of CD24 and CD61, but not of CD49f (Fig. 4B), and also with the tumorsphere formation efficiency (Fig. 4C), suggesting that high ERK activity suppresses the cancer stem cell property. The failure to suppress ERK activity in vivo urged us to use J3B1 cells, which are derived from the non-tumorigenic murine EpH4 mammary epithelial cell line [27]. We found that PD0325901 suppressed ERK activity and increased the expression of CD24 and CD61 (Supplementary Fig. S4), indicating that ERK negatively regulated the expression of CD24 and CD61. Again, CD49f expression was not affected by the decrease in the ERK activity. Altogether, these observations are compatible with the proposal that high ERK activity suppresses the cancer stem cell property in the MMTV-Neu mammary tumor model.

Previous studies have identified CD24, CD49f, and CD61 as markers of the mammary stem cells and/or luminal progenitor cells [28-31]. The identified markers have also been used to purify CSCs/TICs in MMTV-Neu mice. Liu *et al*. demonstrated a dramatic increase in the

$CD49f^{+}CD24^{+}$ population in mammary tumors, which efficiently form tumorspheres [25]. In the initial attempt to use CD61 as a CSC/TIC marker, Vaillant et al. did not find significant enrichment of CSCs/TICs in the $CD61^{high}$ population [32]; however, a later study identified the $CD49f^{high}CD61^{high}$-sorted fraction as a TIC-enriched population of MMTV-Neu mice, which displayed increased tumorsphere formation ability, enhanced tumorigenicity in vivo and drug resistance to paclitaxel and doxorubicin [26]. We found that ERK^{high} cells exhibited not only the decrease of cells that were positive for CD49f, CD24, and CD61 but also a decrease of the tumorsphere efficiency in vitro and tumor formation efficiency in the fat-pad injection assay (Fig. 3). Furthermore, ERK activity in mammary tumors inversely correlated with the expression level of CD24 and CD61 and the tumorsphere formation efficiency (Fig. 4). In mouse ES cells, it has been established that ERK activity must be suppressed for the elimination of differentiation-inducing signaling [33]. In agreement with this report, we found that mammary tumor cells with higher ERK activity were selectively eliminated in vitro (Supplementary Fig. S4). Thus, low ERK activity may be beneficial for self-renewal of the CSCs/TICs of mammary tumor cells as in EC cells.

It has been established that ERK plays critical roles in the expansion of CSCs/TICs of breast cancer [6, 10, 11]. Intuitively, this observation would seem to undermine the finding that ERK^{high} cells isolated from mammary tumor tissues were less tumorigenic than ERK^{low} cells (Fig. 3). Previous studies have demonstrated the roles of ERK by comparing cells with and without oncogene expression, indicating that the cancer cell population, on average, shows high ERK activity, rapid cell growth, and enrichment of CSCs/TICs in comparison to control cells. Therefore, it is plausible that, within breast cancer tissues, the cell population with lower ERK activity is enriched in CSCs/TICs and that the cell population with higher ERK activity is enriched in rapidly-expanding and, at the same time, vulnerable cells.

CONFLICT OF INTEREST

The authors declare no conflict of interest.

ACKNOWLEDGEMENTS

J3B1 cells were kindly provided by Roberto Montesano. We thank Y. Inaoka, K. Hirano, K. Takakura, R. Tabata, Y. Kitagawa and A. Kawagishi for their technical assistance. We are grateful to the members of the Matsuda Laboratory for their helpful discussions. MM was supported by a Grant-in-Aid for Scientific Research on the Innovative Area of "Fluorescence Live imaging" (No. 22113002) of the Ministry of Education, Culture, Sports, Science, and Technology (MEXT), and by an Innovative Techno-Hub for the Integrated Medical Bio-imaging Project of the Special Coordination Funds for Promoting Science and Technology by MEXT, Japan. YK was supported by a Grant-in-Aid for JSPS Fellows from MEXT, Japan. The animal protocols were reviewed and approved by the Animal Care and Use Committee of Kyoto University Graduate School of Medicine (No. 10584).

Supplementary Information accompanies the paper on the Oncogene website (http://www.nature.com/onc)".

REFERENCES

1 Visvader JE, Lindeman GJ. Cancer stem cells in solid tumours: accumulating evidence and unresolved questions. *Nat Rev Cancer* 2008; **8:** 755-768.

2 Zhou BB, Zhang H, Damelin M, Geles KG, Grindley JC, Dirks PB. Tumour-initiating cells: challenges and opportunities for anticancer drug discovery. *Nat Rev Drug Discov* 2009; **8:** 806-823.

3 Slamon DJ, Godolphin W, Jones LA, Holt JA, Wong SG, Keith DE *et al.* Studies of the HER-2/neu proto-oncogene in human breast and ovarian cancer. *Science* 1989; **244:** 707-712.

4 Magnifico A, Albano L, Campaner S, Delia D, Castiglioni F, Gasparini P *et al.* Tumor-initiating cells of HER2-positive carcinoma cell lines express the highest oncoprotein levels and are sensitive to trastuzumab. *Clin Cancer Res* 2009; **15:** 2010-2021.

5 Korkaya H, Paulson A, Iovino F, Wicha MS. HER2 regulates the mammary stem/progenitor cell population driving tumorigenesis and invasion. *Oncogene* 2008; **27:** 6120-6130.

6 Chang CJ, Yang JY, Xia W, Chen CT, Xie X, Chao CH *et al.* EZH2 promotes expansion of breast tumor initiating cells through activation of RAF1-beta-catenin signaling. *Cancer cell* 2011; **19:** 86-100.

7 Whyte J, Bergin O, Bianchi A, McNally S, Martin F. Key signalling nodes in mammary gland development and cancer. Mitogen-activated protein kinase signalling in experimental models of breast cancer progression and in mammary gland development. *Breast Cancer Res* 2009; **11:** 209.

8 Guy CT WM, Schaller M, Parsons TJ, Cardiff RD, Muller WJ. Expression of the neu protooncogene in the mammary epithelium of transgenic mice induces metastatic disease. *Proc Natl Acad Sci U S A* 1992 **89:** 10578-10582.

9 Ursini-Siegel J, Schade B, Cardiff RD, Muller WJ. Insights from transgenic mouse models of ERBB2-induced breast cancer. *Nat Rev Cancer* 2007; **7:** 389-397.

10 Jeselsohn R, Brown NE, Arendt L, Klebba I, Hu MG, Kuperwasser C *et al.* Cyclin D1 kinase activity is required for the self-renewal of mammary stem and progenitor cells that are targets of MMTV-ErbB2 tumorigenesis. *Cancer cell* 2010; **17:** 65-76.

11 Izrailit J, Berman HK, Datti A, Wrana JL, Reedijk M. High throughput kinase inhibitor screens reveal TRB3 and MAPK-ERK/TGFbeta pathways as fundamental Notch regulators in breast cancer. *Proc Natl Acad Sci U S A* 2013; **110:** 1714-1719.

12 Mueller H, Flury N, Eppenberger-Castori S, Kueng W, David F, Eppenberger U. Potential prognostic value of mitogen-activated protein kinase activity for disease-free survival of primary breast cancer patients. *Int J Cancer* 2000; **89:** 384-388.

13 McGlynn LM, Kirkegaard T, Edwards J, Tovey S, Cameron D, Twelves C *et al.* Ras/Raf-1/MAPK pathway mediates response to tamoxifen but not chemotherapy in breast cancer patients. *Clin Cancer Res* 2009; **15:** 1487-1495.

14 Bergqvist J, Elmberger G, Ohd J, Linderholm B, Bjohle J, Hellborg H *et al.* Activated ERK1/2 and phosphorylated oestrogen receptor alpha are associated with improved breast cancer survival in women treated with tamoxifen. *Eur J Cancer* 2006; **42:** 1104-1112.

15 Svensson S, Jirstrom K, Ryden L, Roos G, Emdin S, Ostrowski MC *et al.* ERK phosphorylation is linked to VEGFR2 expression and Ets-2 phosphorylation in breast cancer and is associated with tamoxifen treatment resistance and small tumours with good prognosis. *Oncogene* 2005; **24:** 4370-4379.

16 Milde-Langosch K, Bamberger AM, Rieck G, Grund D, Hemminger G, Muller V *et al.* Expression and prognostic relevance of activated extracellular-regulated kinases (ERK1/2) in breast cancer. *Br J Cancer* 2005; **92:** 2206-2215.

17 Kunath T, Saba-El-Leil MK, Almousailleakh M, Wray J, Meloche S, Smith A. FGF stimulation of the Erk1/2 signalling cascade triggers transition of pluripotent embryonic stem cells from self-renewal to lineage commitment. *Development* 2007; **134:** 2895-2902.

18 Chappell J, Sun Y, Singh A, Dalton S. MYC/MAX control ERK signaling and pluripotency by regulation of dual-specificity phosphatases 2 and 7. *Genes Dev* 2013; **27:** 725-733.

19 Greber B, Wu G, Bernemann C, Joo JY, Han DW, Ko K *et al.* Conserved and divergent roles of FGF signaling in mouse epiblast stem cells and human embryonic stem cells. *Cell stem cell* 2010; **6:** 215-226.

20 Goto A, Sumiyama K, Kamioka Y, Nakasyo E, Ito K, Iwasaki M *et al.* GDNF and endothelin 3 regulate migration of enteric neural crest-derived cells via protein kinase A and Rac1. *J Neurosci* 2013; **33:** 4901-4912.

21 Kamioka Y, Sumiyama K, Mizuno R, Sakai Y, Hirata E, Kiyokawa E *et al.* Live imaging of protein kinase activities in transgenic mice expressing FRET biosensors. *Cell Struct Funct* 2012; **37:** 65-73.

22 Nobis M, McGhee EJ, Morton JP, Schwarz JP, Karim SA, Quinn J *et al.* Intravital FLIM-FRET Imaging reveals dasatinib-induced spatial control of src in pancreatic cancer. *Cancer Res* 2013; **73:** 4674-4686.

23 Brown AP, Carlson TC, Loi CM, Graziano MJ. Pharmacodynamic and toxicokinetic evaluation of the novel MEK inhibitor, PD0325901, in the rat following oral and intravenous administration. *Cancer Chemother Pharmacol* 2007; **59:** 671-679.

24 Liu L, Greger J, Shi H, Liu Y, Greshock J, Annan R *et al.* Novel mechanism of lapatinib resistance in HER2-positive breast tumor cells: activation of AXL. *Cancer Res* 2009; **69:** 6871-6878.

25 Liu JC VV, Bader GD, Deng T, Pusztai L, Symmans WF, Esteva FJ, Egan SE, Zacksenhaus E. Seventeen-gene signature from enriched Her2/Neu mammary tumor-initiating cells predicts clinical outcome for human HER2+:ERα- breast cancer. *Proc Natl Acad Sci U S A* 2012; **109:** 5832-5837.

26 Lo PK, Kanojia D, Liu X, Singh UP, Berger FG, Wang Q *et al.* CD49f and CD61 identify Her2/neu-induced mammary tumor-initiating cells that are potentially derived from luminal progenitors and maintained by the integrin-TGFbeta signaling. *Oncogene* 2012; **31:** 2614-2626.

27 Montesano R, Soulie P. Retinoids induce lumen morphogenesis in mammary epithelial cells. *J Cell Sci* 2002; **115:** 4419-4431.

28 Pece S, Tosoni D, Confalonieri S, Mazzarol G, Vecchi M, Ronzoni S *et al.* Biological and molecular heterogeneity of breast cancers correlates with their cancer stem cell content. *Cell* 2010; **140:** 62-73.

29 Stingl J, Eirew P, Ricketson I, Shackleton M, Vaillant F, Choi D *et al.* Purification and unique properties of mammary epithelial stem cells. *Nature* 2006; **439:** 993-997.

30 Shackleton M, Vaillant F, Simpson KJ, Stingl J, Smyth GK, Asselin-Labat ML *et al.* Generation of a functional mammary gland from a single stem cell. *Nature* 2006; **439:** 84-88.

31 Asselin-Labat ML, Sutherland KD, Barker H, Thomas R, Shackleton M, Forrest NC *et al.* Gata-3 is an essential regulator of mammary-gland morphogenesis and luminal-cell differentiation. *Nat Cell Biol* 2007; **9:** 201-209.

32 Vaillant F, Asselin-Labat ML, Shackleton M, Forrest NC, Lindeman GJ, Visvader JE. The mammary progenitor marker CD61/beta3 integrin identifies cancer stem cells in mouse models of mammary tumorigenesis. *Cancer Res* 2008; **68:** 7711-7717.

33 Ying QL, Wray J, Nichols J, Batlle-Morera L, Doble B, Woodgett J *et al.* The ground state of embryonic stem cell self-renewal. *Nature* 2008; **453:** 519-523.

34 Parashurama N, Lobo NA, Ito K, Mosley AR, Habte FG, Zabala M *et al.* Remodeling of endogenous mammary epithelium by breast cancer stem cells. *Stem cells* 2012; **30:** 2114-2127.

35 Aoki K, Matsuda M. Visualization of small GTPase activity with fluorescence resonance energy transfer-based biosensors. *Nature Protoc* 2009; **4:** 1623-1631.

36 Ewald AJ, Brenot A, Duong M, Chan BS, Werb Z. Collective epithelial migration and cell rearrangements drive mammary branching morphogenesis. *Dev cell* 2008; **14:** 570-581.

FIGURE LEDENDS

Figure 1. Heterogeneity in ERK activity as visualized by in vivo FRET imaging. ***A***, The transgenic mice expressing an ERK FRET biosensor EKAREV were reported previously [21]. Founder animals were backcrossed with FVB/N for at least two generations before crossing with MMTV-Neu$^{+/+}$ mice (FVB/N; Jackson's Lab). Mice were anesthetized with 1.5% inhalation of isoflurane (Abbott) at 0.5 L/min. Surgical exposure of a tissue flap containing the mammary gland was performed as described previously [34]. The mammary gland in a twelve-week-old female EKAREV$^{+/-}$ mouse was observed under an IX81/FV1000 inverted microscope equipped with a x30 silicon oil-immersion objective lens (UPLSAPO 30xS; Olympus), which was connected to a Mai Tai DeepSee HP Ti: Sapphire Laser (Spectra Physics). The excitation wavelength was 840 nm. Acquired images were analyzed with MetaMorph

software (Universal Imaging) and Imaris Software (Bitplane AG) as described previously [21, 35]. An XY slice, a scheme, and an enlarged FRET/CFP ratio image are shown. The FRET/CFP ratio image is shown in intensity-modulated (IMD) display mode. In the IMD mode, eight colors from red to blue are used to represent the FRET/CFP ratio, with the intensity of each color indicating the mean intensity of FRET and CFP. The upper and lower limits of the ratio range are shown at the bottom of the figure. The FRET/CFP ratios of myoepithelial cells (Myo, N = 32) and luminal cells (Lumi, N = 90) are shown in the histogram. ***B***, A FRET image of mammary tumors developed in EKAREV$^{+/-}$/MMTV-Neu$^{+/-}$ mice and observed under the 2P microscope. ***C***, The CFP intensity and FRET/CFP value in each primary tumor cell were plotted (N = 50). ***D***, Immunostaining of a mammary tumor. Paraffin-embedded sections were fixed with 4% paraformaldehyde, blocked with 3% BSA, incubated with an anti-phosphor-ERK antibody (1:200; cat. no. 4370S; Cell Signaling), and further incubated with Alexa 546-conjugated anti-rabbit IgG (1:1000; no.A-11035; Life Technologies). The section was imaged under a fluorescent microscope. ***E***, Mammary tumors in EKAREV$^{+/-}$/MMTV-Neu$^{+/-}$ mice were timelapse-imaged for 6 hours under a 2P microscope. Red or blue lines represent the time courses of the top or bottom 12.5% of cells (five cells each). P value was calculated using a two tailed Student's t test.

Figure 2. Timelapse in vivo imaging of ERK activity in EKAREV$^{+/-}$/MMTV-Neu$^{+/-}$ mice treated with an MEK or a tyrosine kinase inhibitor. The primary tumors in EKAREV$^{+/-}$/MMTV-Neu$^{+/-}$ mice and the secondary tumors in syngeneic mice were observed by 2P microscopy. ***A***, A MEK inhibitor, PD0325901, was injected intravenously (5 mg/kg) at time zero. The white-boxed regions are magnified in the right panels. ***B***, FRET/CFP ratios of individual cells were plotted against time. The red and blue lines indicate cells belonging to the top and bottom 12.5%, respectively, at the beginning of imaging (N =40). ***C* and *D***, An EGFR/HER2 dual tyrosine kinase inhibitor, Lapatinib, was injected intravenously (50 mg/kg)

at time zero. Data were obtained as in ***A*** and ***B*** (N =40). Error bars indicate SD. *Scale bars*, 20 μm.

Figure 3. Characteristics of the ERK^{high} and ERK^{low} populations. Mammary tumors were dissected from $EKAREV^{+/-}$/MMTV-$Neu^{+/-}$ mice to obtain a single-cell suspension essentially as described previously [36]. Briefly, a portion of the tumor was minced into small pieces with sterile scissors, washed in PBS, digested in collagenase/trypsin for 30 min at 37°C with occasional mixing, and washed once with DMEM/F12 (Life Technologies). Mammary epithelial cells were enriched by Mouse Epithelial Cell Enrichment kit (StemCell Technologies). Single-epithelial cell suspensions were resuspended in L-15 Medium (Life Technologies) and analyzed and/or sorted with a FACSAria (Becton Dickinson). ***A***, Representative FACS dots plots showing the biosensor-expressing mammary tumor cells developed in $EKAREV^{+/-}$MMTV-$Neu^{+/-}$ mice. Mammary tumor cells in the highest and lowest decile with respect to the FRET/CFP ratio were named the ERK^{high} and ERK^{low} populations, respectively. The sorted ERK^{high} and ERK^{low} cells were re-analyzed for the validation of the sorting (shown in red and blue histograms, respectively). ***B***, The ERK^{high} and ERK^{low} cells were plated in poly-HEMA-treated six-well plates (Becton Dickinson) at a density of 10,000 cells/ml in phenol red-free Mammary Epithelial Cell Basal Medium (Takara Bio, Kyoto, Japan) supplemented with 20 ng/ml EGF (Sigma), 20 ng/ml basic fibroblast growth factor (Sigma), 5 μg/ml insulin (Sigma), and 2% B27 supplement (Life Technologies). The tumorsphere formation was evaluated two weeks after plating. The result represents averages of three biological replicates. ***C***, The ERK^{high} and ERK^{low} cells (50 cells each) were injected into fat pads of syngeneic mice. Development of tumors was assessed three months after inoculation. ***D***, Representative flow cytometric profiles for CD24/CD49f or CD61/CD49f were obtained from ERK^{high} and ERK^{low} populations in two representative primary tumors (N = 4). We used anti-CD49f antibody conjugated with Alexa-647 or PE/Cy7 (BioLegend), anti-CD24 antibody conjugated with PE/Cy7 (BioLegend), and anti-CD61 antibody conjugated with Alexa-647

(BioLegend). Error bars indicate S.D. P value was calculated using a two tailed Student's t test.

Figure 4. Inverse correlation of ERK activity with the expression of the cancer stem cell markers. EKAREV$^{+/-}$MMTV-Neu$^{+/-}$ mice bearing mammary tumors were orally administered with 50 mg/kg PD0325901 for one week. Single-cell suspension of tumor cells were prepared as described in the legend to Figure 3. ***A***, Part of cells was subjected to immunoblotting analysis with anti-phospho-ERK antibody or anti-tubulin antibody (Calbiochem). ***B***, Expression of cancer stem cell markers were examined as described in the legend to Fig. 3. Mode values of cells treated with PD0325901 was divided by those without PD0325901 to show the expression level. ***C***, The suspended cells were plated in poly-HEMA-treated six-well plates at a density of 10,000 cells/ml as described in the legend to Figure 3. The tumorsphere formation was evaluated two weeks after plating.

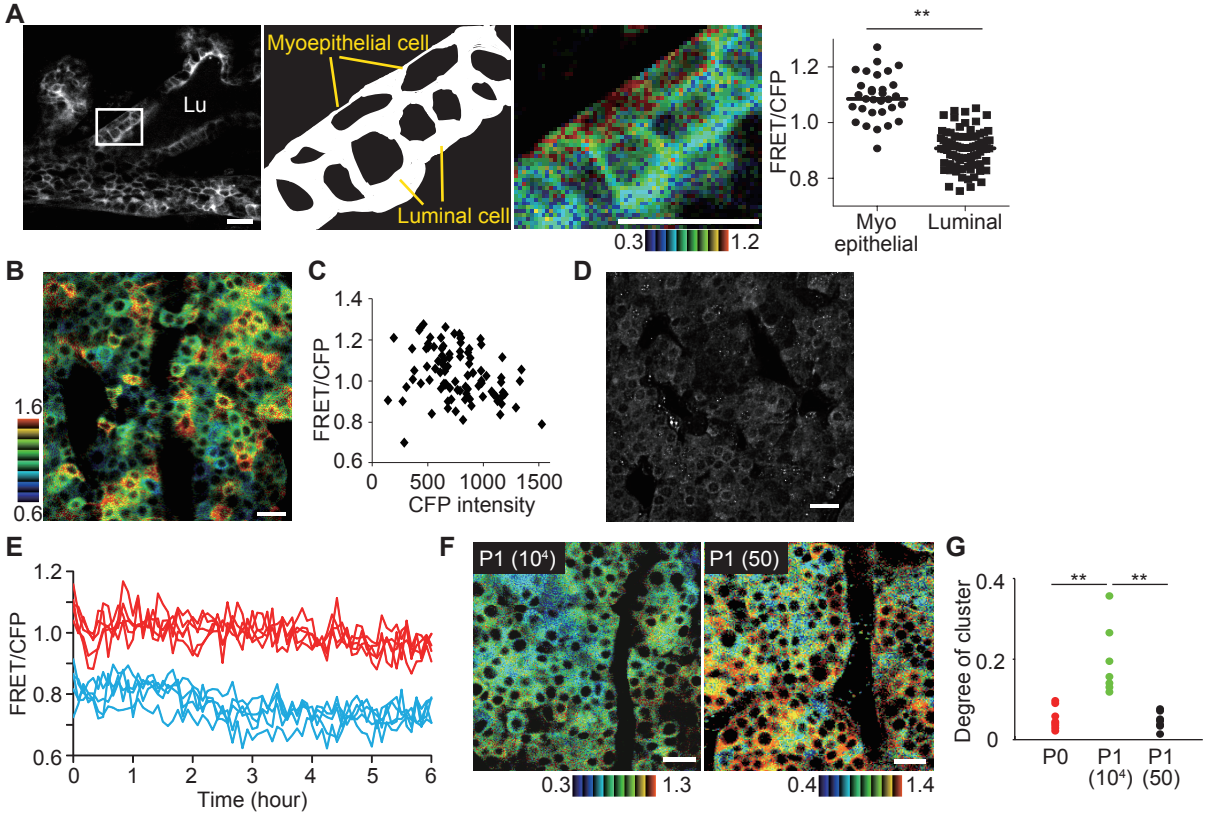
A
Lu
Myoepithelial cell
Luminal cell
0.3
1.2
**
FRET/CFP
1.2
1.0
0.8
Myo epithelial
Luminal
B
1.6
0.6
C
FRET/CFP
1.4
1.2
1.0
0.8
0.6
0
500
1000
1500
CFP intensity
D
E
FRET/CFP
1.2
1.0
0.8
0.6
0
1
2
3
4
5
6
Time (hour)
F
P1 (10⁴)
P1 (50)
0.3
1.3
0.4
1.4
G
**
**
Degree of cluster
0.4
0.2
0
P0
P1 (10⁴)
P1 (50)

Figure 1

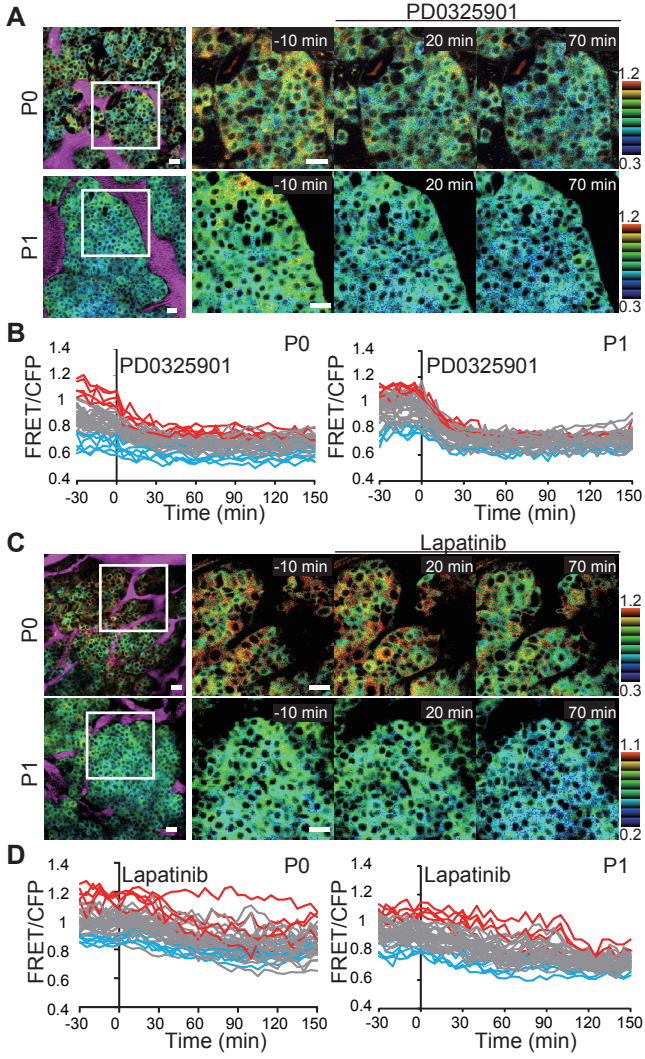
A
PD0325901
P0
P1
-10 min
20 min
70 min
1.2
0.3
1.1
0.2
B
C
D
Lapatinib
PD0325901
FRET/CFP
Time (min)
1.4
1.2
1
0.8
0.6
0.4
-30
0
30
60
90
120
150

Figure 2

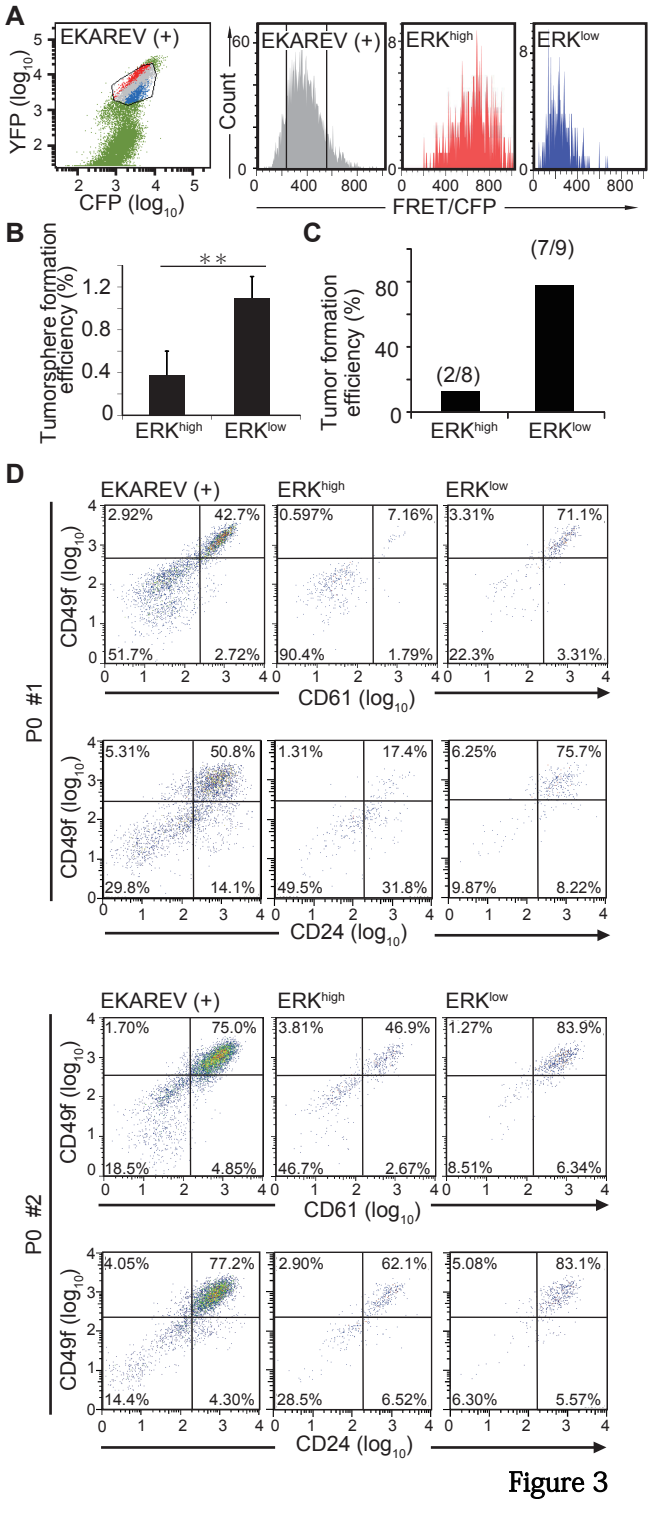
A
EKAREV (+)
YFP (log10)
CFP (log10)
Count
EKAREV (+)
ERKhigh
ERKlow
FRET/CFP
B
Tumorsphere formation efficiency (%)
**
ERKhigh
ERKlow
C
Tumor formation efficiency (%)
(2/8)
(7/9)
ERKhigh
ERKlow
D
P0 #1
EKAREV (+)
ERKhigh
ERKlow
CD49f (log10)
CD61 (log10)
2.92%
42.7%
51.7%
2.72%
0.597%
7.16%
90.4%
1.79%
3.31%
71.1%
22.3%
3.31%
CD24 (log10)
5.31%
50.8%
29.8%
14.1%
1.31%
17.4%
49.5%
31.8%
6.25%
75.7%
9.87%
8.22%
P0 #2
1.70%
75.0%
18.5%
4.85%
3.81%
46.9%
46.7%
2.67%
1.27%
83.9%
8.51%
6.34%
4.05%
77.2%
14.4%
4.30%
2.90%
62.1%
28.5%
6.52%
5.08%
83.1%
6.30%
5.57%

Figure 3

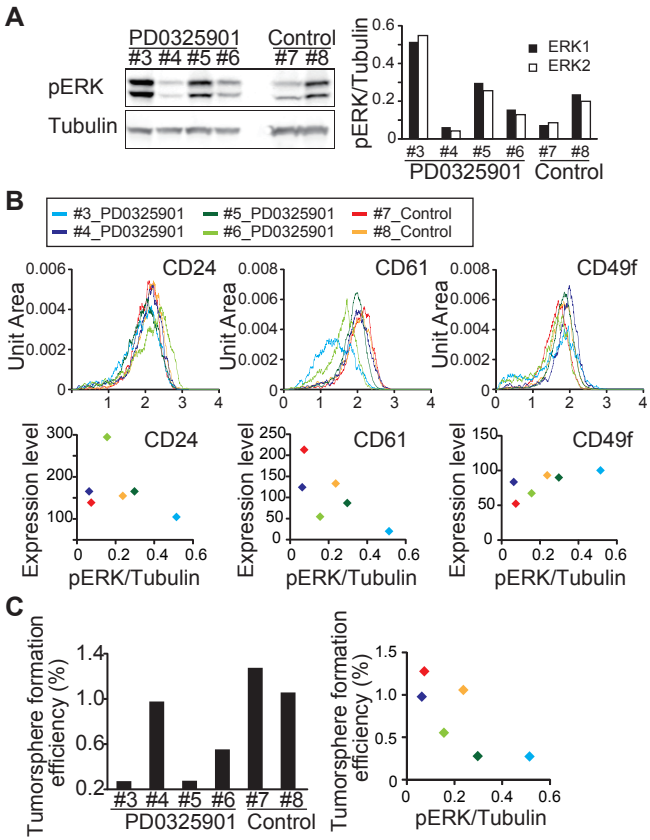
A
PD0325901
Control
#3 #4 #5 #6
#7 #8
pERK
Tubulin
pERK/Tubulin
ERK1
ERK2
PD0325901
Control
B
#3_PD0325901
#4_PD0325901
#5_PD0325901
#6_PD0325901
#7_Control
#8_Control
CD24
CD61
CD49f
Unit Area
Expression level
pERK/Tubulin
C
Tumorsphere formation efficiency (%)
PD0325901
Control

Figure 4

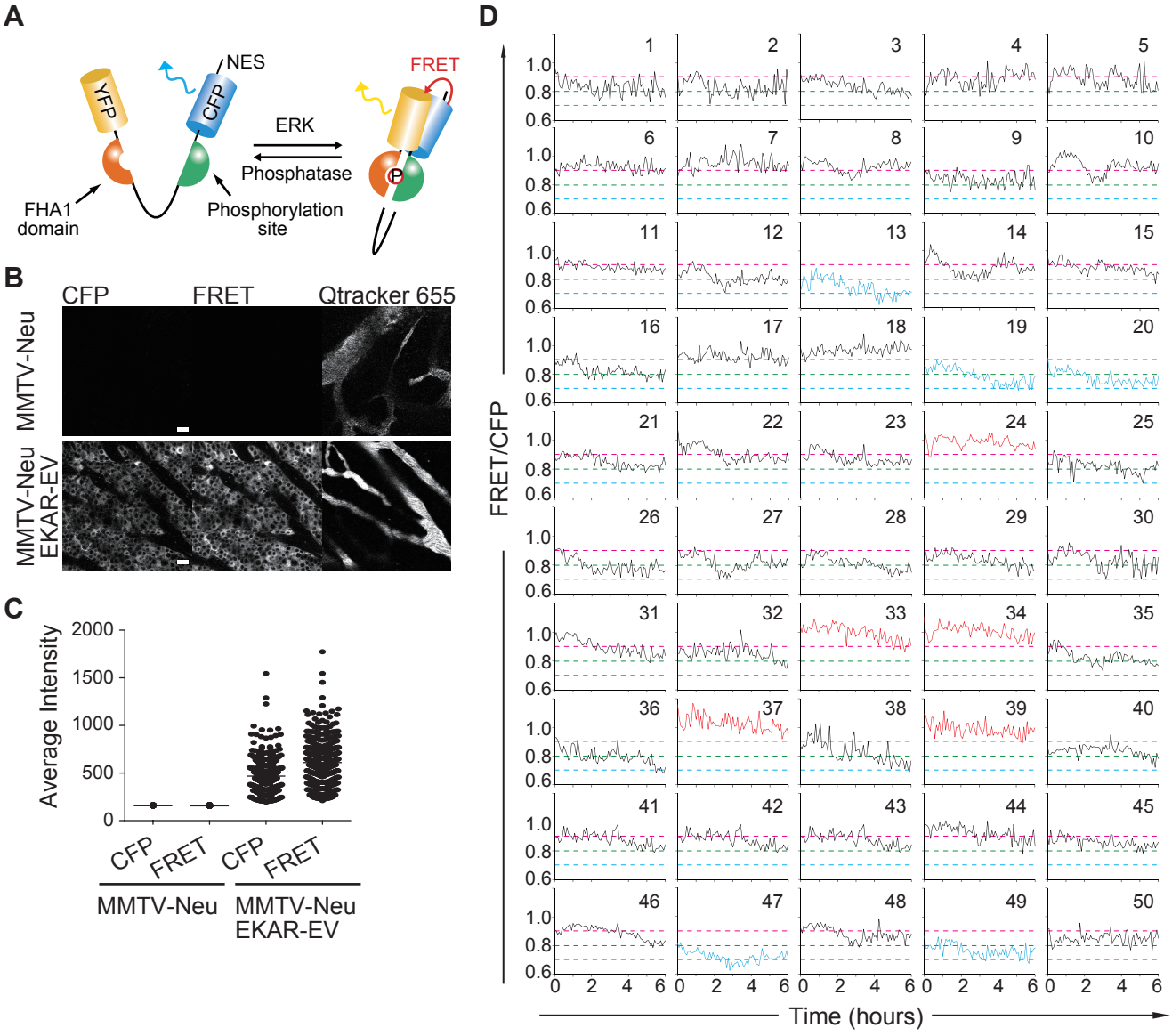

Figure S1. Supplementary information to Figure 1, "Heterogeneity in ERK activity as visualized by *in vivo* FRET imaging."
(A), A FRET biosensor, EAKREV-NES, changes its conformation and increases FRET efficiency upon phosphorylation by ERK. YFP, a yellow fluorescent protein used as a FRET acceptor; CFP, a cyan fluorescent protein used as a FRET donor; FHA1, a phospho-threonine recognition domain; ERK substrates, substrates specific for ERK; NES, nuclear export sequence.
(B and C), A transgenic mice expressing EKAREV and a control FVB/N mice were anesthetized and imaged as described in the legend to Figure 1, except that 10 μl Qtracker 655 was injected intravenously to visualize blood vessels. Images were divided into 506 regions, of which CFP and FRET intensities are shown in panel (C).
(D), Fifty mammary tumor cells in Fig. 1C were timelapse-imaged for 6 hours under a 2P microscope. The red, green, and blue dotted lines indicate the FRET/CFP ratios, 0.9, 0.8, and 0.7, respectively. Panels with red and blue lines are also shown in Fig. 1E. *Scale bar*, 20μm.

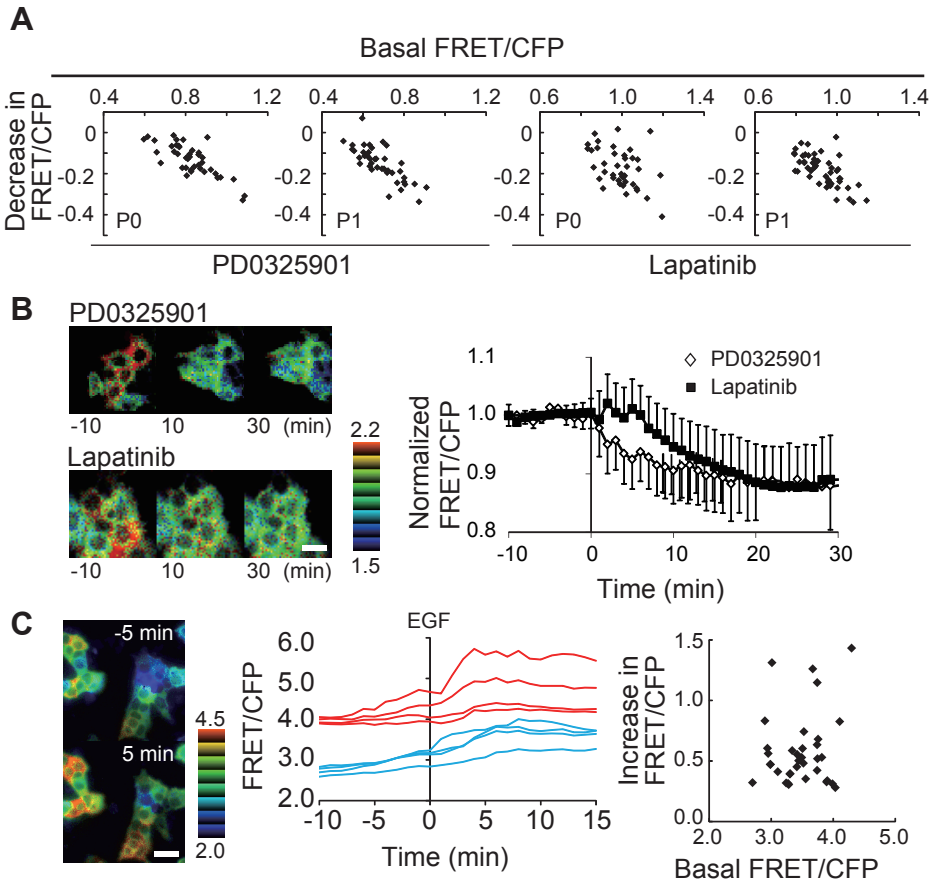

Figure S2. Supplementary information to Figure 2, "Time-lapse *in vivo* imaging of ERK activity in EKAREV$^{+/-}$/MMTV-Neu$^{+/-}$ mice treated with an MEK or a tyrosine kinase inhibitor."
(A), The decreases in FRET/CFP values 90 minutes after intravenous injection of PD0325901 or Lapatinib are plotted against the FRET/CFP values before drug injection.
(B), Response to PD0325901 *in vitro*. Tumor cells were prepared as described in the legend to Figure 3, plated on 35 mm-diameter glass-base dishes, cultured two days in DMEM/F12 containing 5% FBS. Inhibitors, 1 μM PD0325901 or 10 μM Lapatinib, was added at time zero. Cells were imaged at 37oC in 5% CO2 with an inverted microscope (IX81; Olympus, Tokyo, Japan) equipped with a x60 objective lens (PlanApoPH/NA 1.40; Olympus), a cooled CCD camera (Cool SNAP-K4; Roper Scientific, Tucson, AZ), an LED illumination system (CoolLED precisExcite; Molecular Devices, Sunnyvale, CA), an IX2-ZDC laser-based autofocusing system (Olympus) and an MD-XY30100T-Meta automatically programmable XY stage (SIGMA KOKI, Tokyo, Japan). The following filters used for the dual emission imaging studies were obtained from Omega Optical (Brattleboro, VT): an XF1071 (440AF21) excitation filter, an XF2034 (455DRLP) dichroic mirror, and two emission filters, XF3075 (480AF30) for CFP and XF3079 (535AF26) for yellow fluorescent protein (YFP). After background subtraction, FRET/CFP ratio images were created with MetaMorph software (Universal Imaging, West Chester, PA), and represented by intensity-modulated display mode. Error bar indicates S.D. (N = 20).
(C), Response to EGF *in vitro*. Cells were prepared as in (B). EGF (10 ng/ml) was added at time zero. Red and blue lines indicate the time-courses of four cells showing the highest or lowest basal ERK activity. The increases in the FRET/CFP value are plotted against the basal FRET/CFP values. (N = 35) *Scale bar*, 20μm

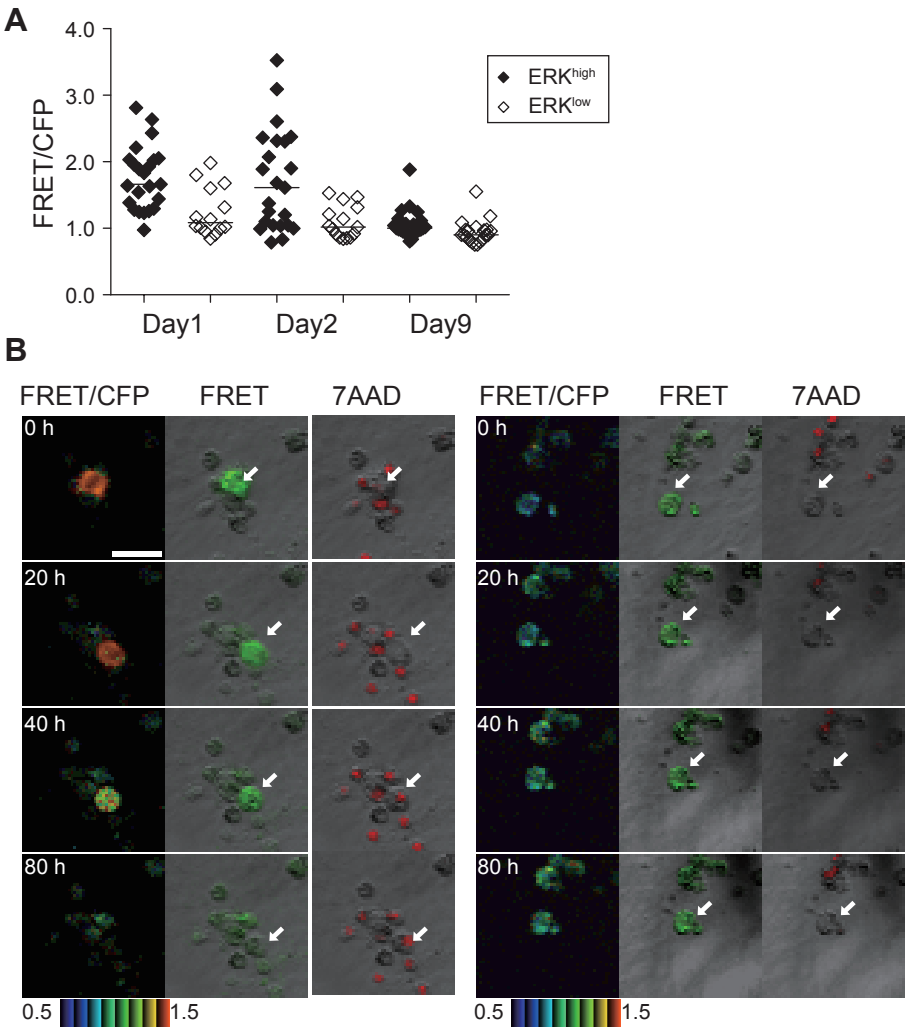

Figure S3. Supplementary information to Fig. 3, "Characteristics of the ERK^{high} and ERK^{low} populations."
(A), ERK^{high} and ERK^{low} cells were prepared as described in the legend to Fig. 3. Cells were embedded in 7.5 mg/ml growth factor-reduced Matrigel (BD), cultured in DMEM/F12 medium containing 5% FBS and imaged with an FV10i laser scanning confocal microscope (Olympus, Tokyo, Japan) for 9 days. The FRET/CFP values at Day 1, 2, and 9 were examined for at least 12 cells in each condition.
(B), Tumor cells before sorting were plated on Matrigel-coated 35 mm-diameter glass-base dishes and cultured in DMEM/F12 containing 5% FBS for 3 days. For the visualization of dead cells, 7AAD (1:200) was included. Cells were imaged with an FV1000 inverted confocal microscope (Olympus, Tokyo, Japan). Arrows are used to show the identical cells. *Scale bar*, 20μm

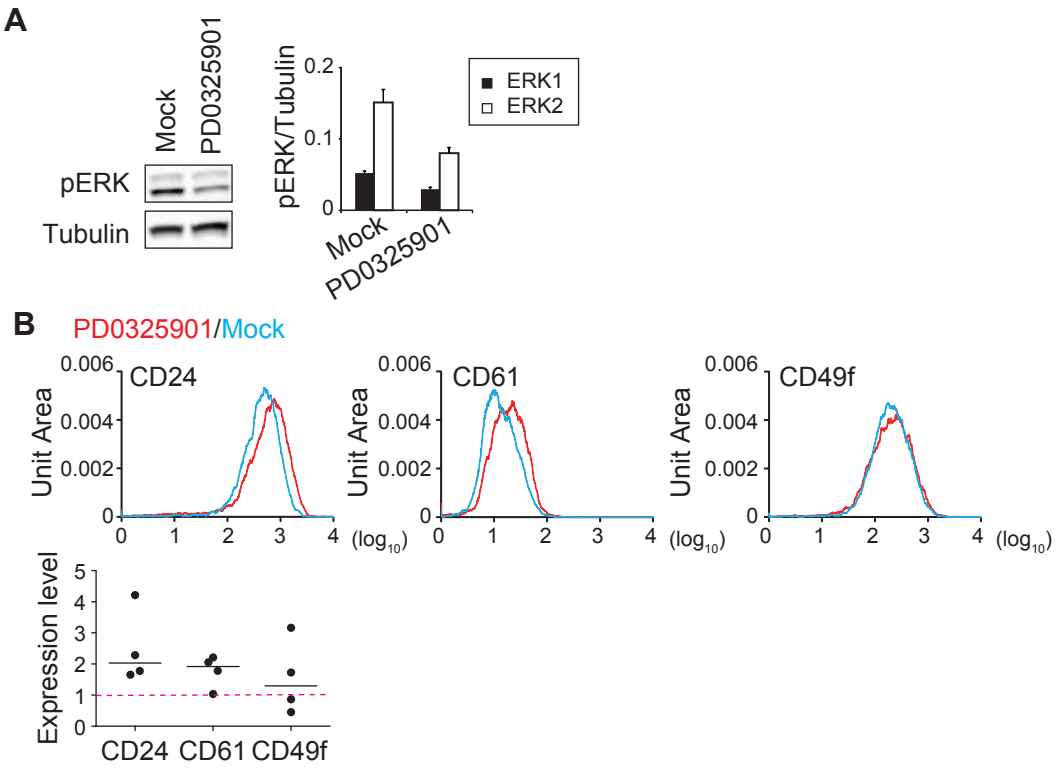

Figure S4. Supplementary information to Fig. 4, "Inverse correlation of ERK activity with the expression of cancer stem cell markers." J3B1 mouse mammary epithelial cells were cultured in the presence or absence of 1 μM PD0325901 for two days.
(A), Part of cells was subjected to immunoblotting analysis with anti-phopho-ERK antibody or anti-tubulin antibody. Error bar indicates S.D. (N = 4).
(B), With the remaining cells, expression of cancer stem cell markers were examined as described in the legend to Fig. 3. Mode values of cells treated with PD0325901 was divided by those without PD0325901 to show the expression level. (N = 4)